J Seismol (2006) 10:315–333
DOI 10.1007/s10950-006-9019-x

ORIGINAL ARTICLE

Ground-motion scaling in the Western Alps

Paola Morasca · Luca Malagnini · Aybige Akinci · Daniele Spallarossa · R. B. Herrmann

Received: 16 September 2004 / Accepted: 15 March 2006

Abstract In order to empirically obtain the scaling relationships for the high-frequency ground motion in the Western Alps (NW Italy), regressions are carried out on more than 7500 seismograms from 957 regional earthquakes. The waveforms were selected from the database of 6 three-component stations of the RSNI (Regional Seismic network of Northwestern Italy). The events, M_W ranging between 1.2 and 4.8, were recorded within a hypocentral distance of 200 km during the time period: 1996–2001. The peak ground velocities are measured in selected narrow-frequency bands, between 0.5 and 14 Hz. Results are presented in terms of a regional attenuation function for the vertical ground motion, a set of vertical excitation terms at the reference station STV2 (hard-rock), and a set of site terms (vertical and horizontal), all relative to the vertical component of station STV2.

The regional propagation of the ground motion is modeled after quantifying the expected duration of the seismic motion as a function of frequency and hypocentral distance. A simple functional form is used to take into account both the geometrical and the anelastic attenuation: a multi-variable grid search yielded a quality factor $Q(f) = 310\,f^{0.20}$, together with a quadri-linear geometrical spreading at low frequency. A simpler, bi-linear geometrical spreading seems to be more appropriate at higher frequencies ($f > 1.0$ Hz). Excitation terms are matched by using a Brune spectral model with variable, magnitude-dependent stress drop: at M_w 4.8, we used $\Delta\sigma = 50$ MPa. A regional distance-independent attenuation parameter is obtained ($\kappa_0 = 0.012$ s) by modelling the average spectral decay at high frequency of small earthquakes.

In order to predict the absolute levels of ground shaking in the region, the excitation/attenuation model is used through the Random Vibration Theory (RVT) with a stochastic point-source model. The expected peak-ground accelerations (PGA) are compared with the ones derived by Ambraseys et al. (1996) for the Mediterranean region and by Sabetta and Pugliese (1996) for the Italian territory.

Keywords Attenuation · Ground motion · Western Alps

P. Morasca (✉) · D. Spallarossa
DIPTERIS, Universita' di Genova, Viale Benedetto XV, 5, 16132 Genova, Italy
e-mail: alpocc@dipteris.unige.it

L. Malagnini · A. Akinci
INGV, Viale di Vigna Murata 605, 00143 Roma, Italy

R. B. Herrmann
Dept. of Earth and Atmo. Scie. of Saint Louis University

Introduction

Many studies show that the ground motion levels are quite different in zones of different tectonic regimes such as extensional and compressional (Boore et al., 1997; Campbell, 1997; Sadigh et al., 1997; Atkinson

and Silva, 1997; Atkinson and Boore, 1995), and this has an influence on the seismic hazard evaluations.

This has been taken into account in the new seismic hazard map that has been recently produced in Italy by a National Working Group. In fact they used the regionalized predictive relationships for the ground motion that were already available for part of the Italian territory: the Eastern Alps, Malagnini et al. (2002) the Apennines, Malagnini et al. (2000a) Malagnini and Herrmann (2000) and Sicily, Scognamiglio et al. (2005). Since a regional attenuation function for the northwestern Italy has never been developed, the present study represent an important contribution to the completeness of the national hazard model.

Besides covering the entire Italian territory with specific regional predictive relationships, two other important motivations exist for this study: the first one is to get the ability of correcting the Fourier spectra of regional earthquakes for the contribution of the crustal propagation; the second one is about the interpretation of the regional propagation in terms of the gross, azimuthally-averaged, characteristics of the crust down to the Moho.

As for the first point understanding the regional wave propagation is crucial for predicting earthquake-induced ground motions. For this reason, the determination of quality factor Q, source parameters and site amplification is an important goal of seismic analysis in seismology. Aim of this study is to calibrate attenuation parameters specifically for the western Alps using a large amount of weak-motion recordings. In fact the application of the previous relationships by Sabetta and Pugliese (1996) or Ambraseys et al. (1996) to the western Alps data may lead to wrong results since they are based on strong motion data recorded in a variety of regions, while the western Alps are known as a region of moderate seismicity.

As for the second point, we should keep in mind that the western Alps are a complex structural region characterized by strong lateral variations (Cattaneo et al., 1999; Kissling, 1993; Kissling and Spakman, 1996) that influence the thickness of the crust with important effects on the propagation within the region. The interpretation of the regional propagation is an important contribution in the understanding the complexity of this region. We try to do this by comparing our attenuation results with other studies in the alpine range.

Another important aim of this study is to obtain moment magnitudes through an automatic procedure that apply our calibrated attenuation parameters to correct for path effects. This represent a useful contribution for a future routine seismic moment determination within a region characterized by moderate seismicity.

Finally we want to define a relationship between seismic moment and local magnitudes for the western Alps. Although a previous relationship was calibrated in a similar range of magnitude by Lanza et al. (1999) for a small sector of southwestern Alps, our goal is to define it on a regional scale so that the relation may be useful also for future earthquakes occurring within the western Alps.

For accomplishing this tasks we analyzed a large data set from the background seismicity, relative to small-to-moderate events occurred in the western Alps region.

Tectonic and geologic setting

Different kinematic styles exist in Italy, as a result of the complex geodynamic processes that have conditioned the build-up of the Alpine and Apennine chains. The continent-continent convergence between the African and the Eurasian plates during the Alpine orogeny has been responsible for the formation of the Alps, that are mainly characterized by compressional and transpressional structures (e.g. CNR-PFG, 1987; Castaldini and Panizza, 1991; Galadini et al., 2001; Dewey et al., 1973; Polino et al., 1990). The Alps are composed of two folded chains, with opposite orogenic polarity, separated by the Insubric lineament, a major E-W-trending tectonic element. The North-alpine chains are built by a pile of nappes in a sandwich-like structure, where the intermediate oceanic units are enclosed between the underlying European units and overlying African units (Dal Piaz, 1995). Large and thick portions of the crystalline basement of both continental margins are involved in the structures, such as the Helvetic massifs in the Western Alps and lower Austroalpine nappes in the Eastern Alps. The structure of the Southern Alps is a south-verging thrust belt involving the Permian to Tertiary cover and, partly, the underlying Hercynian crystalline basement (Castellarin, 2001).

Results derived by seismic tomography in the study region (Paul et al., 2001; Kissling, 1993; Kissling and Spakman, 1996) suggest that the Western Alps display strong lateral variations both at shallow and deeper levels determining significant effects on the

propagation of seismic wavefields. The Ivrea body is an important feature of the region, and represents a high-velocity anomaly (Kissling, 1993; Di Stefano et al., 1999) interpreted as a mantle slice whose effect masks deeper structures (Paul et al., 2001) and creates difficulties for the waveform modeling. At a regional scale, a high-velocity anomaly beneath the Po plain and the northern Apennines has been interpreted as subducting European slab (Kissling and Spakman, 1996).

As a consequence of the structural complexity of the Western Alps, it is very difficult to precisely define the depth of the Moho beneath the region (Cattaneo et al., 1999; Kissling, 1993; Kissling and Spakman, 1996). The thickness of the crust seems to be affected by strong lateral variations, and ranges from about 10 km in the Ligurian Sea to nearly 50 km beneath the Alps (Buness et al., 1990). A bathymetric map of the Moho, proposed by Kissling (1993) for the Western Alps, does not give us a complete 3D model, although it evidences the asymmetry of the crustal roots of the region, and suggests a separation of the crust-mantle boundary into three surfaces: the European, the Adriatic and the Apenninic Moho.

The seismic activity of the region is generally moderate (Cattaneo et al., 1999; Eva and Solarino, 1998; Sue et al., 1999), with most of the events within the first 20 km in depth, even though Cattaneo et al. (1999) evidenced the presence of earthquakes characterized by large focal depths. The 23 February, 1887, magnitude 6.3 earthquake was the greatest seismic event in the area in the last thousand years (Ferrari, 1991).

Description of the data set

The area is monitored by the RSNI (Regional Seismic network of Northwestern Italy), managed by the Seismological Group of DipTeRis-GS (Dipartimento per lo studio del Territorio e delle sue Risorse, Sezione Geofisica). At present, the network consists of 29 stations, partially located in the Western Alps and partially in the Northern Apennines (Lunigiana-Garfagnana region): 12 of them are one-component short-period stations, connected via telephone analog telemetry (not used in this study). The other 17 stations are equipped with digital three-component seismometers (Guralp CMG40 and Lennartz LE3D-5s), characterized by a 126-dB dynamic range. Particularly, the Lennartz LE3D-5s has a flat frequency response in a range from 0.2 to 40 Hz and the CMG40 has a flat velocity response in a range from 0.033 to 50 Hz. The acquisition procedure is performed by a dial-up LennartzMars88 MC system provided with a 20 bit A/D converter (ADSP).

We selected more than 7500 recordings from 957 regional earthquakes recorded in the Western Alps by the six three-component digital stations located in the region (the other three-component stations are located in the Northern Apennines), during a time period of 1996–2001 (see Fig. 1 and Table 1). The bulk of the data set is made from events of magnitude lower than 3 (Fig. 2A and 2B), but seismograms from earthquakes of larger magnitude, up to $M_W = 4.8$, are also included.

Although a local magnitude calibrated for Northwestern Italy by Spallarossa et al. (2002) was available, for our dataset we dispose of moment magnitudes computed by Morasca et al. (2005). As discussed by the authors their coda-derived moment magnitudes are very stable, and for this reason we decided to use those values for all our analysis. The relation between the two magnitudes is described in their Figure 7b.

The distribution of the focal depths (Figure 2D) shows that the data set consists mainly of shallow events, with only a few ones deeper than 15 km. Figure 3 shows three cross sections that will help understanding the spatial distribution of the events in the data set. The AA′ and CC″ cross sections in Figure 3 approximately follow the geometrical structure of the Briançonnais and the Piedmont arc that are characterized by focal depths between 0 and 20 km, respectively. The BB″ cross section clearly shows an increase of the focal depths from west to east, involving deep structures. The apparent increase of focal depths between 200 and 220 km on the BB′ cross section is probably an artifact of the location procedure.

Figure 4 shows the distribution of hypocentral distances of all the available seismograms. The spatial sampling of our recordings is fairly homogeneous, up to hypocentral distances of about 160 km, although there is a larger concentration of events around 50 km (Fig. 2C). The distance range covered by each station is generally fairly wide, since about 650 events of the data set were recorded at all stations. Finally, Figure 5 presents the signal-to-noise (S/N) ratios for our data set calculated in the frequency band between 2.0 and 11.0 Hz, using a time window of 2 sec.

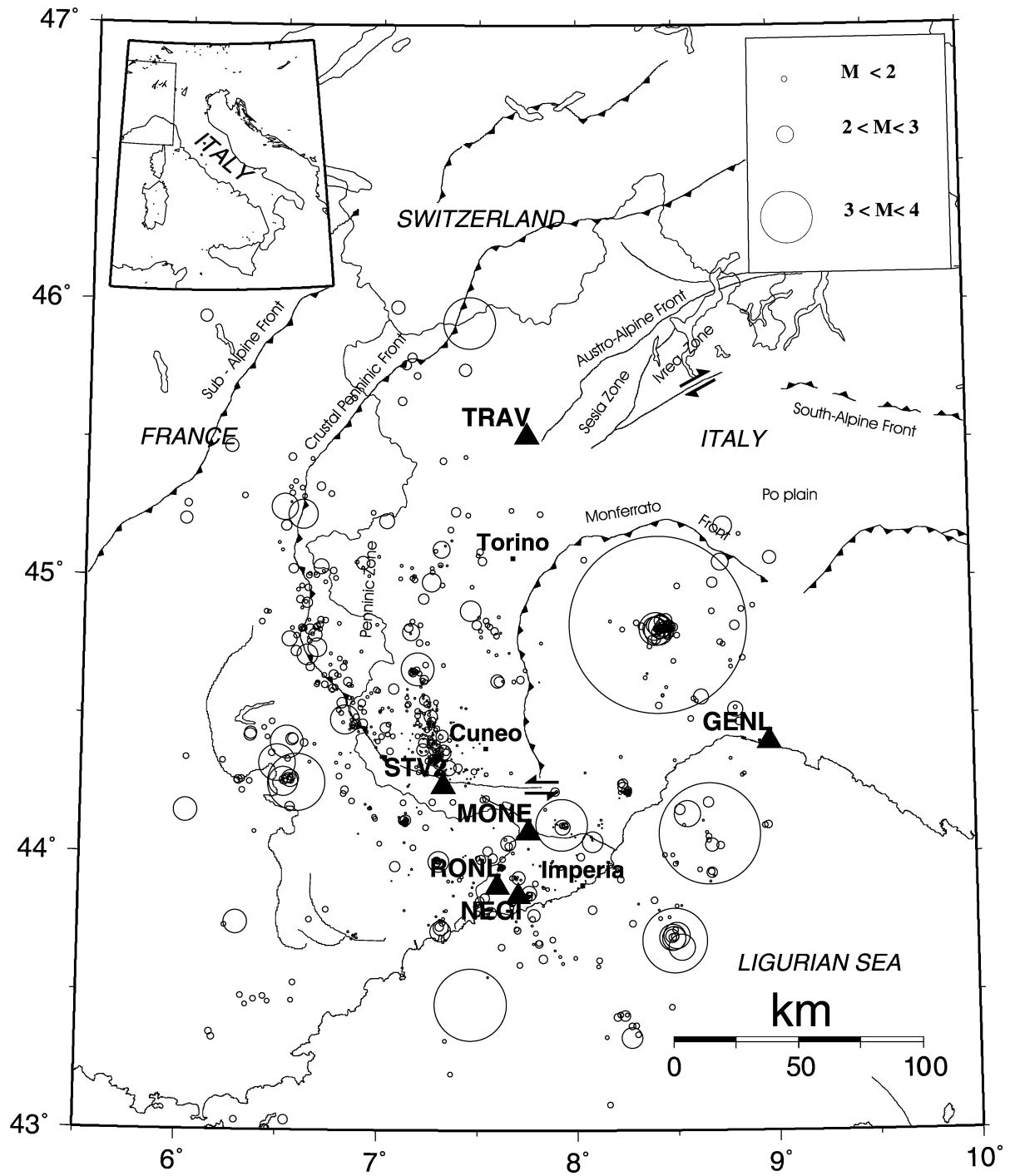

Fig. 1 Events and stations used in this study. The main seismic activity in the Western Alps is concentrated along an external belt, corresponding to the Crustal Penninic Front (CPF), and along an internal belt, corresponding to the border of the Penninic zone and the Po plain. These seismic belts are connected with a westward translation of the West-Alpine arc and of the Po plain that drives the observed seismicity mechanism (Giglia et al., 1996; Sue et al., 1999; Sue and Tricart, 1999)

Table 1 Three-component stations used in this study

Station code	Latitude	Longitude	H (m)	Sensor	Acquisition system	Notes
GENL	44N24.34	08E58.18	80	Guralp CMG40	Lennartz Mars88 MC	Since 1995
MONE	44N04.77	07E45.30	1320	Guralp CMG40	Lennartz Mars88 MC	Since 1991
NEGI	43N50.86	07E42.23	640	Guralp CMG40	Lennartz Mars88 MC	Since 03/1996
TRAV	45N30.76	07E44.82	990	Guralp CMG40	Lennartz Mars88 MC	Since 1996
STV2	44N14.73	07E19.56	930	Guralp CMG40	Lennartz Mars88 MC	Since 1996
RONL	44N52.88	07E35.89	300	Lennartz LE3D-5s	Lennartz Mars88 MC	Since 01/1999

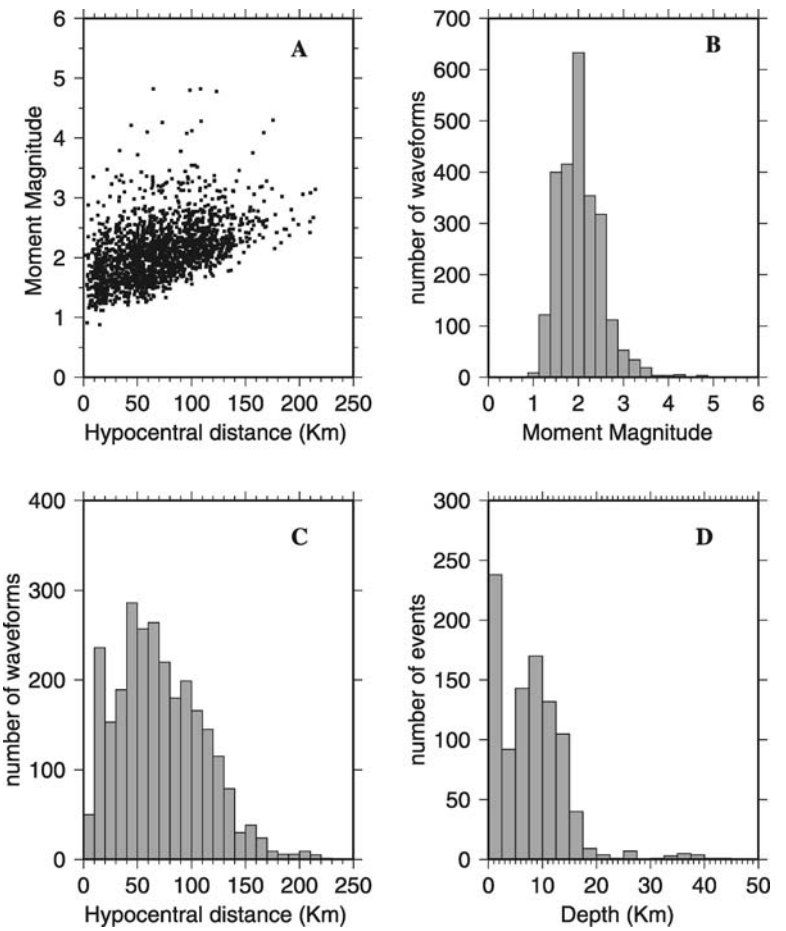

Fig. 2 Characteristics of the data set. (A) Distribution of moment magnitude (Morasca et al., 2005) with respect to hypocentral distance; (B) Number of waveforms as a function of moment magnitude. The bulk of the events used in this study is characterized by M_W lower than 3, although we included recordings from earthquakes up to $M_W = 4.8$; (C) Number of recordings as a function of hypocentral distance; (D) Distribution of the event depths, showing that the data set consists mainly of shallow events

Method and data analysis

In this section, we will briefly review the procedure used for the data processing. For a more detailed description of the method, we refer the reader to the papers by Malagnini et al. (2000b, 2002).

The original waveforms, corrected for the instrument response, were bandpass-filtered around a set of 14 sampling frequencies between 0.5 and 14 Hz. Each filter, chosen the central frequency f_c, was obtained by using an 8-pole highpass Butterworth filter with corner frequency at $1/\sqrt{2}f_c$, followed by an 8-pole lowpass Butterworth filter with corner at $\sqrt{2}f_c$. (see Malagnini et al., 2000b). The peak value of each filtered time history (both horizontal and vertical components) is measured and a check of the signal-to-noise ratio is performed. Peaks smaller than three times the rms amplitude of the pre-event noise are rejected.

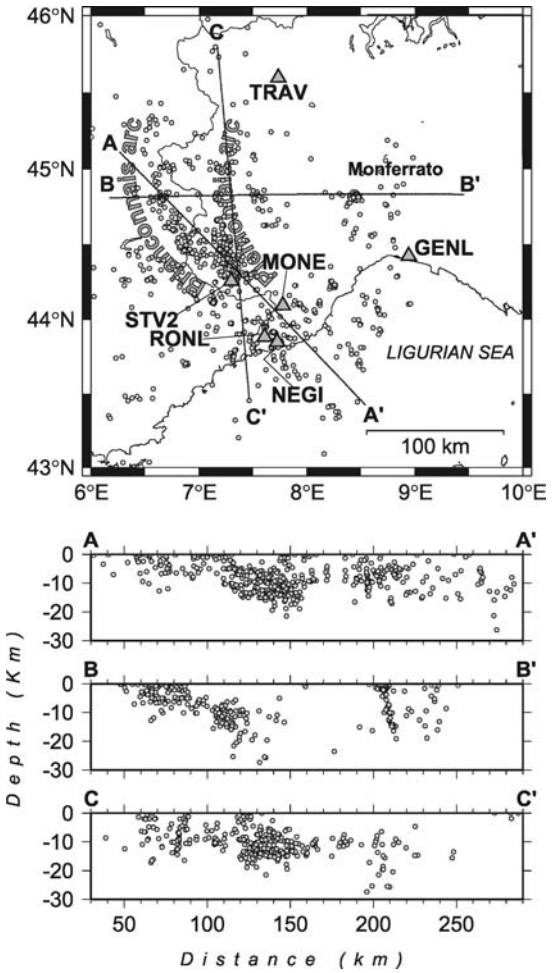

Fig. 3 Seismicity cross-section through the western Alps: the AA″ and CC″ sections try to follow the geometrical structure of the internal and external arcs. The BB″ section shows that focal depths are deeper from west to east

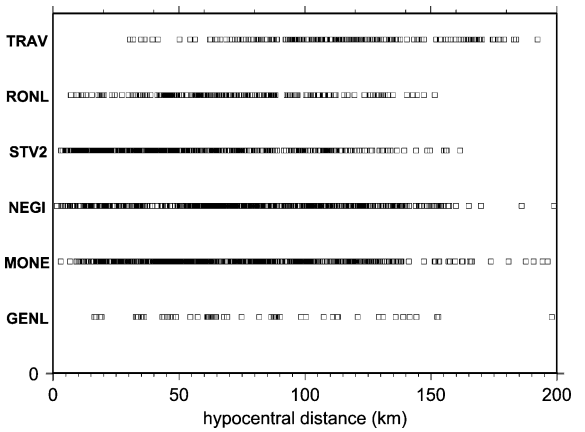

Fig. 4 Distance coverage for the three components stations used in this study. Each square in this figure represents one distinct three-component seismogram. The spatial sampling of our recordings is fairly homogeneous up to hypocentral distances of about 160 km

Regressions are carried out on the time domain bandpass-filtered peak ground velocities, after casting in matrix form the thousands available observations at each sampling frequency. The matrix form is indicated in the following scheme:

$$A_k(f_0, r_{ij}) = \mathrm{SRC}_i(f_0, r_{\mathrm{ref}}) + \mathrm{SITE}_j(f_0) + D(r_{ij}, r_{\mathrm{ref}}, f_0) \quad (1a)$$

where $A_k(f_c, r_{ij})$ is the logarithm of the observed peak amplitude (j-th station, i-th event) for the k-th waveform band-pass filtered around f_0; $D(r_{ij}, r_{\mathrm{ref}}, f_c)$ is described with a piecewise continuous function:

$$D(r_{ij}, r_{\mathrm{ref}}, f_0) = \sum_{m=1}^{N} L_m(r_{ij}) D_m \quad (1b)$$

where $L_m(r)$ is a linear function, and D_m is the value of the attenuation function at the hypocentral distance, r.

For stability, the following constraints are applied during the regression analysis:

$$\bullet\ D(r = r_{\mathrm{ref}}, f) = 0\ (r_{\mathrm{ref}} = 40\,\mathrm{km}) \quad (2)$$

Constraint (2) maps source effects to an arbitrary reference distance. To facilitate comparisons with the results of similar studies elsewhere in Italy (Malagnini et al., 2002), we chose the reference distance to be 40 km.

$$\bullet\ \mathrm{SITE}_{\mathrm{STV2(Z)}}(f) = 0 \quad (3)$$

Because of constraint (3), all site terms are relative to the hard-rock station STV2, that is deployed on gneiss outcrops of the Argentera Massif. The excitation terms, $\mathrm{SRC}_i(f_0, r_{\mathrm{ref}})$, are also related to this specific reference station.

- A smoothing constraint is also applied to D (r, r_{ref}, f):

$$D_{j-1}(f) - 2D_j(f) + D_{j+1}(f) = 0 \quad (4)$$

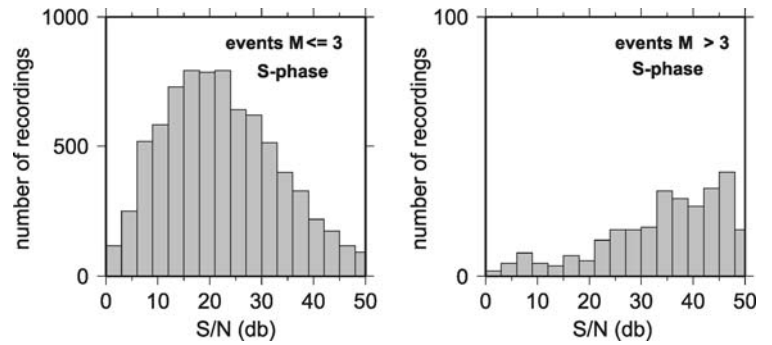

Fig. 5 Signal-to-noise (S/N) ratios calculated in the frequency band 2–11 Hz on a window of 2 s

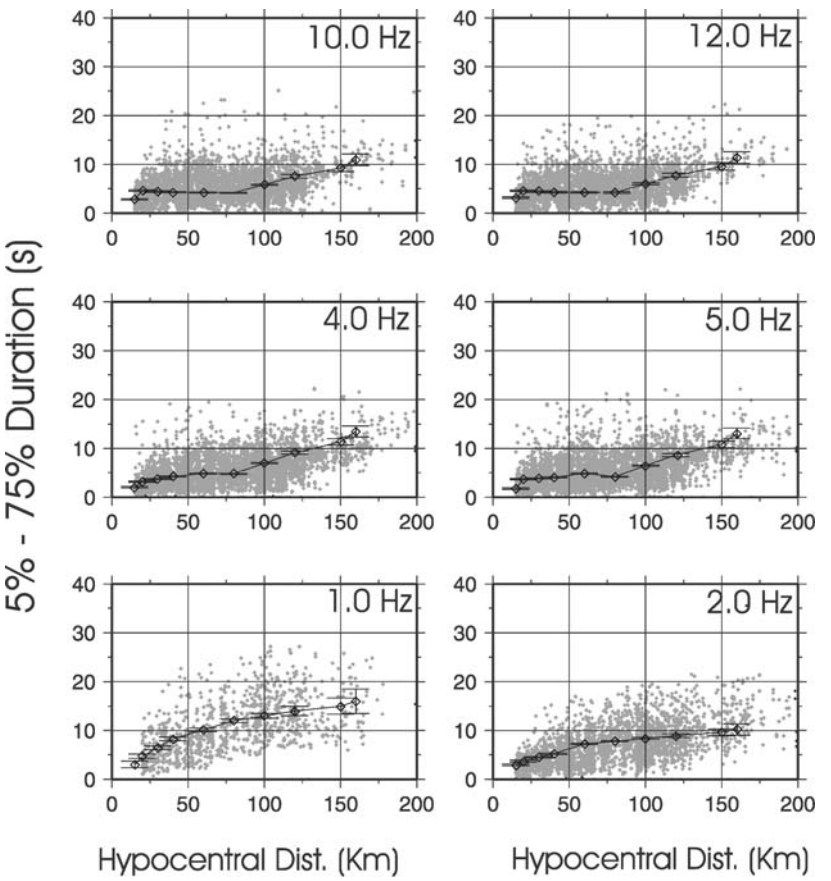

Fig. 6 Duration distribution for the regional data at different frequencies. It is computed on each individual recording in the data set as the time window bracketing the 5–75% of the integrated seismic energy that follows the S-wave-onset. Small grey diamonds indicate individual values of duration; large black diamonds indicate the average estimates of the duration computed at a set of nodes. The error bars were estimated using a least-squares inversion algorithm

Equation (4) describes a minimum roughness constraint, which equals a null-second derivative when the nodes are evenly spaced.

The processing is the same for horizontal and vertical components except for the site term since the STV2 vertical site is forced to zero and the horizontal and the other vertical site terms are left free to vary. This imply that the excitation and propagation terms are referred to the vertical motion observed at the station STV2.

Duration of the ground motion is calculated for each seismogram. At each frequency, duration is defined as the length of the time windows comprising the 5–75% of the energy following the S-wave arrivals on the filtered seismograms. Figure 6 shows the observed durations and the inverted values together with the errors indicated by the vertical bars at all frequencies. The uncertainties are generally small, and increase for distances larger than 150 km because of the small number

of observations. We estimate the duration of each seismogram, and check its reliability by comparing the observed peak motion to its RVT prediction (via the Stochastic Model SIMulation code – SMSIM – Boore, 1996).

Results

Attenuation model for the region

We modeled the empirical estimates of the peak amplitudes, as a function of hypocentral distance in each frequency band. Since the crustal attenuation is described as a combination of geometrical spreading $g(r)$, and a frequency-dependent crustal attenuation parameter, $Q(f)$, $D(r, r_{\text{ref}}, f)$ can be described as following equation:

$$D(r, r_{\text{ref}}, f_c) = \log\, g(r) - \log\, g(r_{\text{ref}}) - \frac{\pi f_c (r - r_{\text{ref}})}{\beta Q_0 (f/f_{\text{ref}})^{\eta}} \log\, e; \quad (5)$$

The search on the parameters Q_0 and η in: $Q(f) = Q_0(f/f_{\text{ref}})^{\eta}$ ($f_{\text{ref}} = 1.0\,\text{Hz}$), and on the geometrical spreading function $g(r)$ in (5) yielded:

$$Q(f) = 310 f^{0.20} \quad (6)$$

$$g(r) \propto \begin{cases} r^{-0.9} & r \le 40\,\text{km} \\ r^{-0.5} & 40 < r \le 100\,\text{km} \\ & 0.5\,\text{Hz} \le f \le 1.0\,\text{Hz} \\ r^{-0.9} & 100 < r \le 120\,\text{km} \\ r^{-0.5} & r > 120\,\text{km} \end{cases}$$

$$g(r) \propto \begin{cases} r^{-0.9} & r \le 40\,\text{km} \\ & f > 1.0\,\text{Hz}\ c \\ r^{-0.5} & r \le 40\,\text{km} \end{cases} \quad (7)$$

Although (in the log log space) Equation (7) describes a quadri-linear geometrical spreading for the lower frequency band ($0.5\,\text{Hz} \le f \le 1.0\,\text{Hz}$), the high-frequency term ($f > 1.0\,\text{Hz}$) given by Equation (8) is simply bilinear, with a body-wave-like spreading ($g(r) \sim 1/r$) out to 40 km (hypocentral distance), and cylindrical spreading ($g(r) \propto 1/\sqrt{r}$) beyond 40 km. Figure 7 shows the empirical function describing the crustal attenuation in the Western Alps, as obtained from the regressions on the peak values of the band-pass filtered ground velocities. Grey curves represent the empirical estimate of the term $D(r, r_{\text{ref}}, f)$ at various frequencies, while the black curves represent theoretical predictions obtained using Equations (6)–(8). Although for $f = 2$, 3 and 4 Hz the models overestimate the observations at large distances, for all other cases a good fitting is obtained. Observing the error bars we have an idea of the accuracy of the estimates. For low frequencies we note larger errors because most events are small in our dataset. However for all other frequencies results are more stable at all distances.

Comparisons with results of studies in the alpine range

For the Italian Alps some comparisons about the crustal attenuation term $Q(f) = Q_0 f^{\eta}$, and/or with the high-frequency geometric attenuation $g(r)$, which contains information about the crustal velocity structure, can help to better understand the tectonic regime of the region.

Some comparisons with the results by Bay et al. (2003), on Switzerland and by Malagnini et al. (2002), on the eastern Alps are appropriate for our results because they used the same methodology. However, although different approaches are applied by other authors, it is interesting to analyze their results for the alpine range.

For the eastern Alps, various attenuation functions have been proposed (Castro et al., 1996; Console and Rovelli, 1981; Malagnini et al., 2002). Although some of these studies use a different approach, a strong frequency dependence was observed by all the authors. At low frequencies differences in the anelastic attenuation are insignificant, but the high-frequency wave propagation is apparently a lot more efficient in the eastern Alps. The Q_0 terms indicated by Castro et al. (1996) and Console and Rovelli (1981), are lower than in the western Alps, (20.4 and 80 respectively) while Malagnini et al. (2002), used a more similar Q_0 (i.e. 260). This is probably due to the fact that we use the same method and take into account of a complex geometrical spreading having a role in the trade-off existing between this term and the anelastic attenuation. However, Malagnini et al. (2002) found a more complex apparent geometrical spreading than in the Western Alps, with branches steeper than $1/r$ (almost as steep as $1/r^2$) at intermediate

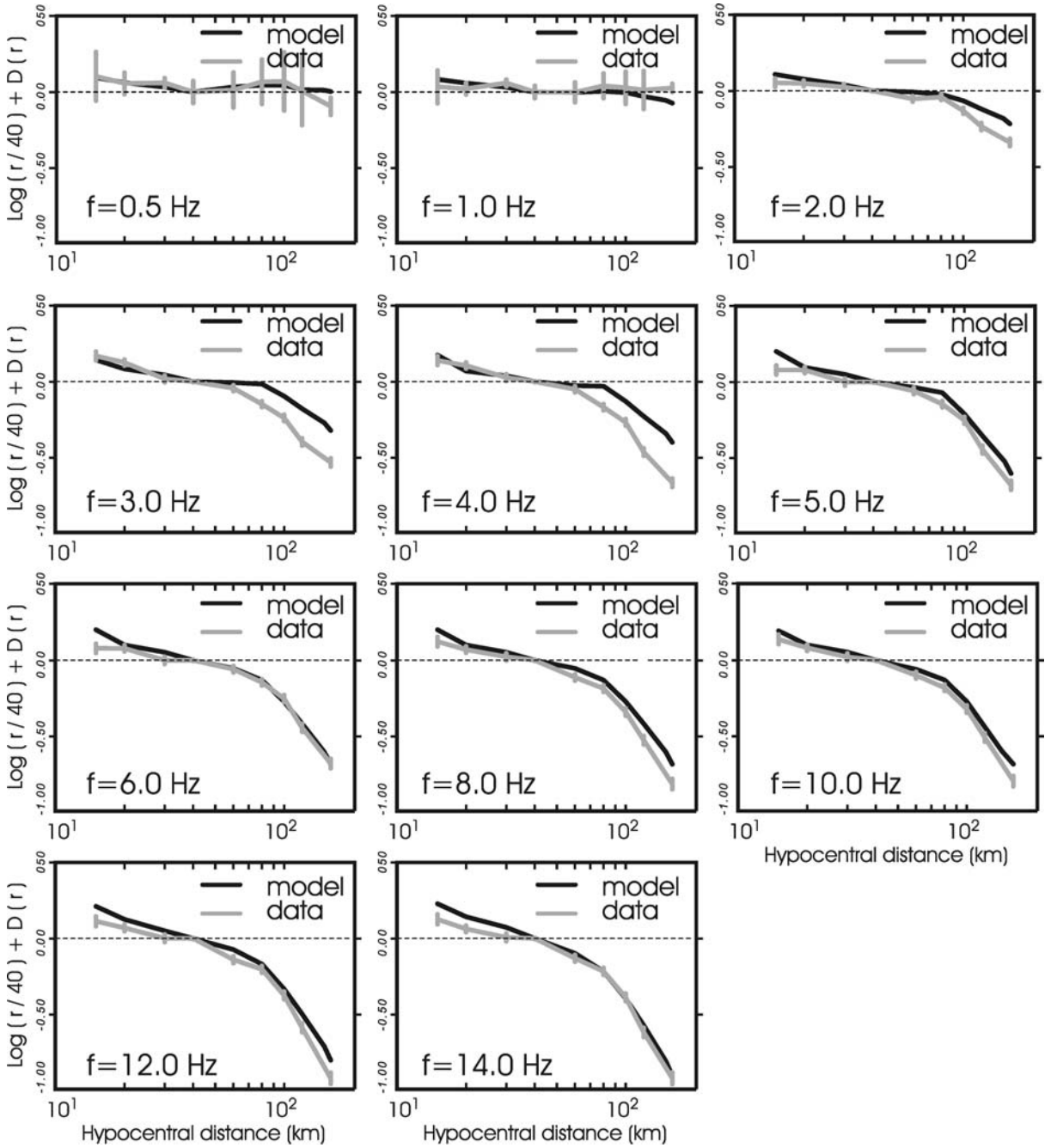

Fig. 7 Attenuation functional $D(r,f)$ obtained, for western Alps, from the regressions on the filtered velocities at the frequencies indicated in the figure. Grey curves represent the final regression results, the black lines describe the theoretical predictions. Attenuation curves are normalized to zero at the reference hypocentral distance of 40 km. For plotting purposes only we normalized the amplitude decays to $1/r$ for the term $D(r, r_{\mathrm{ref}}, f)$. Thus, horizontal curves in the figure really decay as $1/r$. This choice increases the visual spread of curves at different frequencies, and allows a better sensitivity on the frequency dependence, η, of the attenuation function

distances, that may be interpreted as shadow zones due to velocity inversions at depth. The nature of this peculiar behavior is related to the compressive tectonic setting of the eastern Alps, where the present tectonics acts via low-angle, northward-dipping thrust faults.

Swiss Alps were recently investigated by Bay et al. (2003). After using the same method as in this study, they indicated the following crustal parameters: $Q(f) = 270 f^{0.50}$. Their results are more similar to the ones obtained for the eastern Alps by Malagnini et al. (2002) than for the ones of this study. A complex, quadri-linear (in a log log space) geometrical spreading was proposed for Switzerland, where spherical propagation characterizes short distances (less than 50 km), cylindrical propagation takes over beyond 100 km, and a complex pattern exists between the two crossover distances. A deeper Moho beneath the Swiss Alps explains the farther transition to cylindrical propagation, and the large crustal shortening experienced by the central Alps during their tectonic history has probably leaded to a more complex average 1-D vertical layering than for the western Alps.

Using a different methodology Thouvenot (1983) analyzed the quality factor for the Central Alps and its frequency dependence in the range 10–25 Hz. He obtained different Q models for different depths within the upper crust, with Q_0 values between 83 and 756 using an exponent of 0.25. Although we used natural earthquakes and Thouvenot (1983) obtained his results analyzing explosions and defining the quality factor for compressional waves, the models are comparable. In fact our $Q_0 = 320$ represent an average over the depth, assuming a frequency dependence of 0.20. Our frequency dependence parameter is valid also for lower frequencies than those considered by Thouvenot (1983).

The features of regional variation of coda Q were studied by Eva et al. (1991) for the Western Alps. They found coda Q values characterized by strong lateral variations related to the structural complexity of the area. Usually the cristalline massifs showed higher coda Q values than the central stretching zone. Our method cannot resolve these features, but can only provide us with the best median crustal attenuation model.

Source excitation spectra

The empirical excitation terms $\mathrm{SRC}_i(f_0, r_{\mathrm{ref}})$ are modeled using the Brune (1970) spectral model, then they

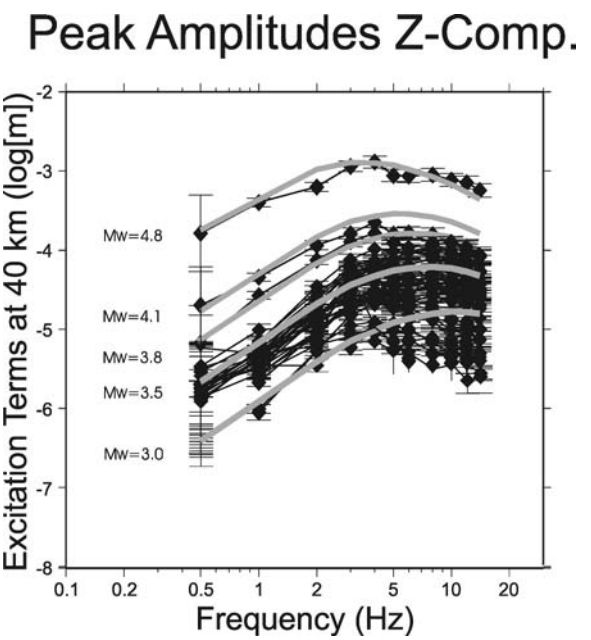

Fig. 8 Comparison between empirical excitation terms obtained from the regressions (indicated by the black diamonds linked by thin black lines) and the predictions from different moment magnitudes, obtained by using the RVT (thick gray lines). Error bars are associated at each empirical term

are "propagated" to the reference hypocentral distance of 40 km (Equations (5)–(8)). Figure 8 shows the empirical excitation terms obtained for the peak filtered amplitudes (black diamond linked by thin black lines). Notice that the error bars are quite large at low frequencies. The thick gray lines in the figure refer to the theoretical excitation terms obtained by using Equations (5)–(11) at various moment magnitudes:

$$\mathrm{exc}(f, r_{\mathrm{ref}}) = s(f, M_W) g(r_{\mathrm{ref}}) \exp\left[-\frac{\pi r_{\mathrm{ref}}}{\beta Q_0 (f/f_{\mathrm{ref}})^{\eta}}\right] \times V(f) \exp(-\pi f \kappa_0) \quad (8)$$

where $V(f) = 1.0$:

$$s(f, M_W) = K \frac{M_{\mathrm{o}}}{4\pi\rho\beta^3 1000} (2\pi f) S(f) \quad (9)$$

$$K = 0.24 \quad (10)$$

The constant parameter K in Equations (10) and (11) (Boore, 1983, 2000; Atkinson and Boore, 1995) takes into account: (i) the radiation pattern, log- or rms-averaged over a suitable range of azimuth and take off angles ($\langle R_{\Theta\Phi} \rangle$, Boore and Boatwright, 1984); (ii)

Table 2 Parameters of the Brune spectrum used to compute the theoretical excitation terms

ρ	2.8 g/cm^3
β	3.5 km/s
$\Delta\sigma_{(M_w=4.8)}$	50 Mpa
$\Delta\sigma_{(M_w=4.1;\,M_w=3.8)}$	45 Mpa
f_c	$4.9 \times 10^6 \beta\,(\Delta\sigma/M_0)^{1/3}$ Hz
κ_0	0.012 s
$\nu(f)$	1.0

the amplification due to the free surface, and (iii) the partitioning of energy into horizontal components. Although we have no information to separate each contribution, we have the necessity to calibrate K to the specific dataset using independent information (Herrmann and Malagnini, 2005). We thus defined this parameter on our dataset using independent and stable moment magnitudes given in a recent source study on the same dataset (Morasca et al., 2005).

The reference distance has been selected so that it is far enough from source to minimize depth errors, but not too far for reflected crustal arrivals to complicate the motion (Herrmann and Malagnini, 2005). In Table 2 we report the numerical values of all parameters of the spectral model. The term, $\exp(-\pi\kappa_0 f)$, is used to model the decay of the high-frequency band in the empirical excitation spectra. In our formulation, κ_0 is a distance-independent site term, related to the effective anelastic absorption at shallow depths beneath station STV2 of the vertical ground motion carried by S-waves (the only station and component of the ground motion constrained to be zero during the regressions).

Since the stress parameter in the Brune model trades off with κ_0, we need to calibrate κ_0, and then to quantify the stress parameter $\Delta\sigma$ by best-fitting the excitation terms. As seen in Figure 9, the high-frequency spectral amplitudes of small events are essentially dominated by the effect of κ_0 and for large events, a strong trade-off exists between κ_0 and the stress parameter $\Delta\sigma$. We estimated $\kappa_0 = 0.012$ s by fitting the shape of the average spectrum of about 130 small earthquakes. The stress drop is thus calculated from the largest events in our data by fixing $\kappa_0 = 0.012$ s, and the values are indicated in Table 2.

Site terms and H/V ratios

Vertical and horizontal site terms obtained from our regressions and H/V ratios are shown in Figure 10. Since we forced the vertical site term at station STV2 to be zero during the inversions, all individual (vertical and/or horizontal) site terms given here are relative to the STV2 vertical-component motion.

The empirical site term, $\mathrm{SITE}_j(f)$ has the following meaning:

$$10^{\mathrm{SITE}_j(f)} = \frac{V_j(f)\exp(-\pi\kappa_{0j}f)}{V_{\mathrm{STV2}}(f)\exp(-\pi\kappa_{\mathrm{STV2}}f)} \tag{11}$$

The regional high-frequency term:

$$\exp(-\pi\kappa_0 f) \approx V_{\mathrm{STV2}}(f)\exp(-\pi\kappa_{\mathrm{STV2}}f) \tag{12}$$

$V_j(f)\exp(-\pi\kappa_{0j}f)$; $V_j(f)$ is the site-specific elastic response, and $\exp(-\pi\kappa_{0j}f)$ is the distance-independent, site-specific, high-frequency anelastic attenuation. From a visual inspection of the Figure 10, we see that the error bars tend to be larger at 0.5 Hz. The same result is obtained for the empirical attenuation $D(r, r_{\mathrm{ref}}, f)$ in Figure 7, for which large standard-deviation error bars are observed at low frequency. This is due to the fact that our dataset is mainly composed by small-to-moderate events.

Figure 10 also reveals that the entire set of site terms is characterized by some fluctuations with respect to the vertical STV2. Station MONE, shows a substantial amplification on the horizontal components of the ground motion, in the 1–14 Hz frequency band. This result was expected because MONE is located on the debris of a paleolandslide while STV2 is on gneissic rocks. Moreover, a relative site effect between these two stations was observed by Spallarossa et al. (2002) for the same frequency band. For the other four stations, the poor knowledge of the shallow geology makes the interpretation difficult. However, as stated by Spallarossa et al. (2002), probably station TRAV is located on hard rock, and in fact our results show in general small fluctuation for this station. GENL, RONL and NEGI seem to amplify at high frequency, and this could be explained as an effect of impedance contrast and/or resonance.

The residuals of the regressions are shown for each frequency band in Figure 11 using a logarithmic scale to amplify the outliers. The behavior is nearly Gaussian for all cases, and the number of large residuals is generally lower than few tens for each frequency. Skewness

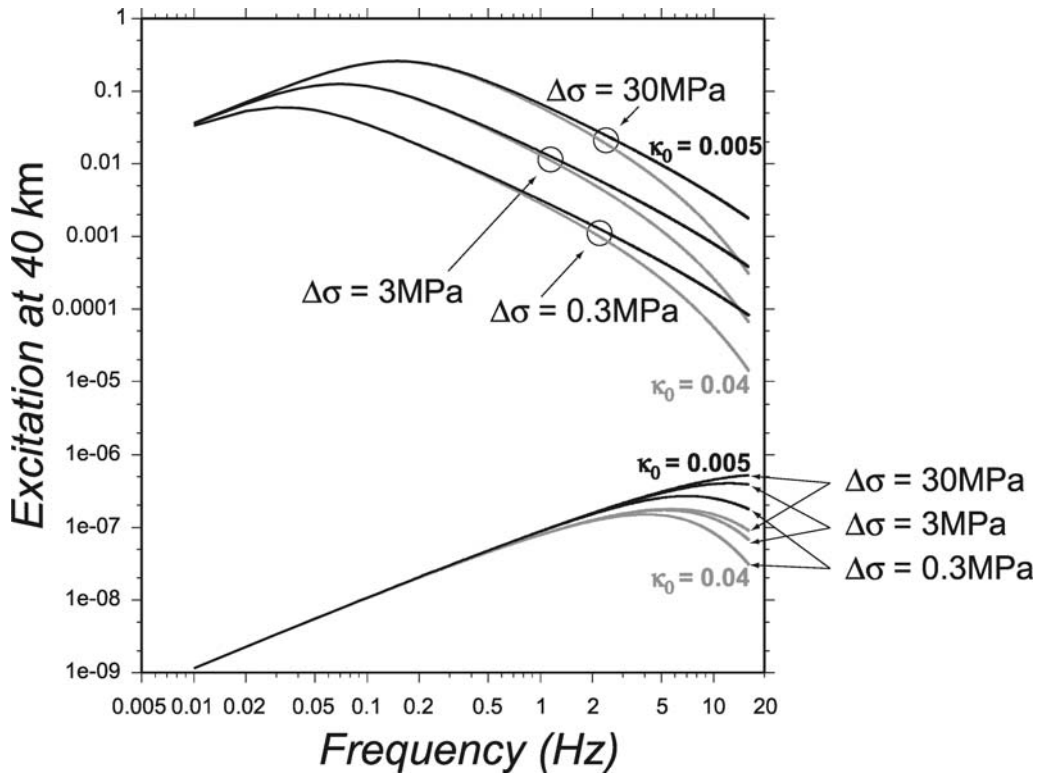

Fig. 9 As an example we show velocity spectra for $M_w = 2$ and 7 obtained through the Brune spectral model with three different values for the stress parameter and using two values for the high frequency attenuation parameter (κ_0). Gray curves have been derived using $\kappa_0 = 0.04$ (value generally associated with moderately attenuating sites) while black curves using $\kappa_0 = 0.005$ (usually referred to rock sites). The figure shows the influence of κ_0 on the high-frequency amplitudes of small events, and the tradeoff between κ_0 and the stress parameter for large earthquakes. For this reason, it is necessary first to find estimates of the high frequency parameter, κ_0, on small events spectra, and than, knowing κ_0, of the stress parameter of the larger events

is observed in all distributions relative to frequencies $f \geq 3$ Hz.

Automatic moment magnitude calibration

Through a completely automatic procedure, Malagnini et al. (2004) use the regionally-calibrated attenuation parameters obtained from similar regressions in the eastern Alps in order to compute corrected moment-rate spectra for small and moderate earthquakes. Similarly, in this paper we compute seismic moments from the rms-average of the flat portion of the corrected moment-rate spectra of the events in the data set, and thus the moment magnitudes for all the events in our data set.

Independent values of M_W were also computed by Morasca et al. (2005) for all the events in the data set, based on measurements taken on the seismic coda, that are much less sensitive to the source radiation pattern and to 3D-heterogeneities than our direct phase measurements, we calibrated the constant K on their moment magnitudes. As shown in Figure 12a, using $K = 0.24$ in (10), our results are comparable to the ones of Morasca et al. (2005). This means that, in the Western Alps, the effect of complex structures, lateral heterogeneities, and irregularities close to the surface, have an important influence on the average values described by K. For this parameter, in the eastern Alps, Malagnini et al. (2004) used the canonical value: $K = 0.89$. The standard deviations relative to our estimates are of the order of 0.2 (Fig. 12 b). The comparison with Morasca et al. (2005), also show that the effects of the heterogeneous distribution of stations on the regression parameters has been taken into account.

Finally, Figure 12c shows our seismic moments versus the local magnitudes computed by Spallarossa et al. (2002) for all data. The thick black line is the result of

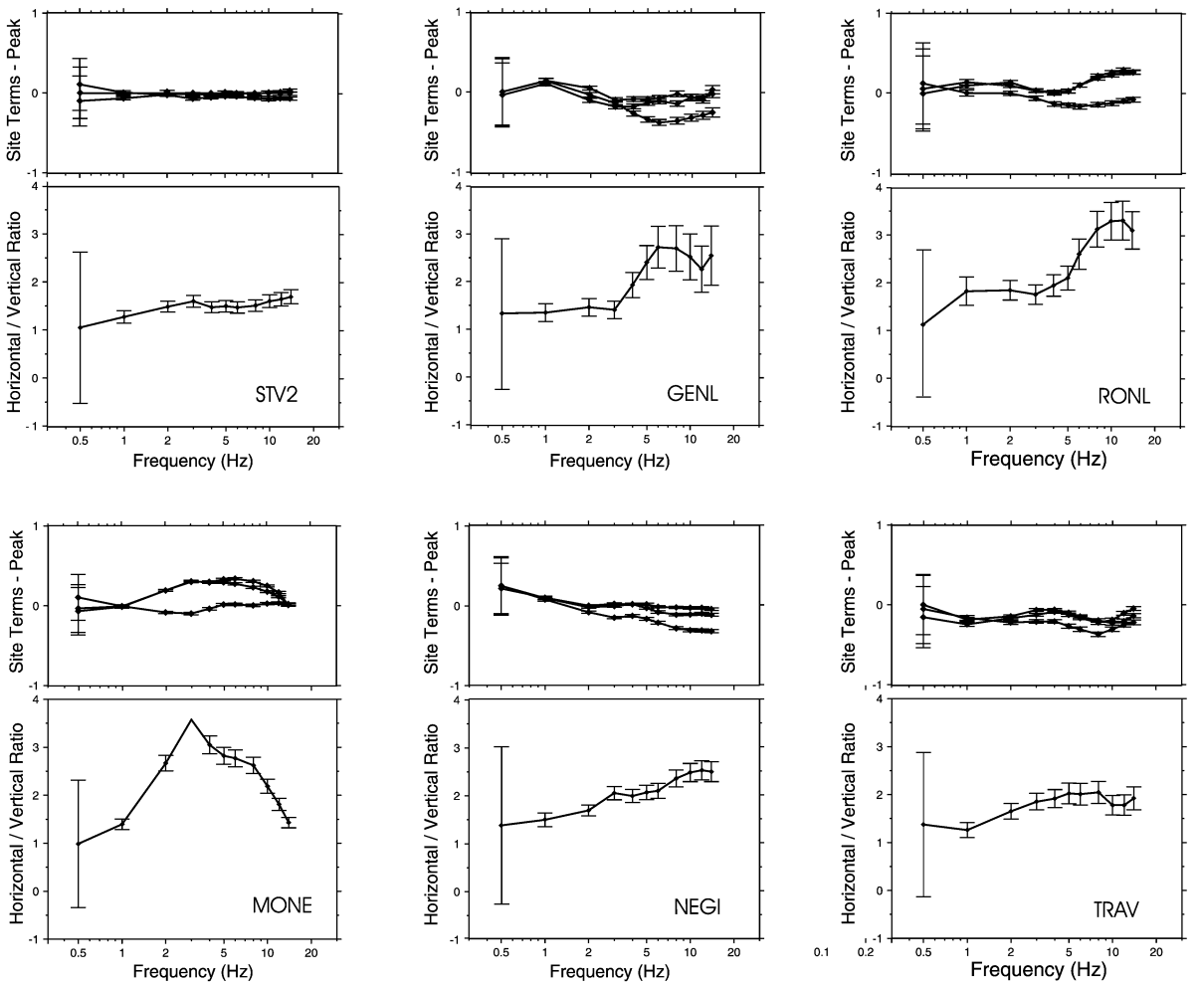

Fig. 10 Inverted site terms for the regressions over the peak values and H/V ratio for each station. We forced STV2 to be zero, during the regressions, because it is on a hard rock location, consequently each site term refers to STV2. Error bars are plotted to indicate the standard deviations associated at each frequency for all stations

the data least-square fitting. It is described by the following moment versus magnitude relationship:

$$\log M_0 = (0.92 \pm 0.01) M_L + (17.676 \pm 0.007) \quad (13)$$

It is worth mention that there is no specific physical meaning for the relationship above to be linear, unless within a very narrow magnitude range.

The magnitude range of confidence is between 0.5 $\leq M_L \leq$ 5.1. We also compared our results with the relations of Scherbaum and Stoll (1983) for the Swabian Jura, SW Germany (Log M_0 = 1.05 M_L + 16.86, 1.0 $\leq M_L \leq$ 4.5), Granet and Hoang Trong (1980) for Friuli, NE Italy (Log $M_0 = 0.83\, M_L + 17.40$, $0.8 \leq M_L \leq 3.0$), and Lanza et al. (1999) for the Southwestern sector of Alps (Log $M_0 = 1.06\, M_L + 16.94$, $1.5 \leq M_L \leq 4.5$). Our relationship (14) shows a clear DC-shift relative to these studies. Scherbaum and Stoll's moments are based on 5 sites over approximately 1 km of sediment, and they computed moments from the 1–10 Hz bandpass, with no corrections for site amplifications. Local magnitudes derived by Spallarossa et al. (2002) are calibrated on the same area analyzed in this study. The relationship by Lanza et al. (1999) was calculated by using data recorded during two swarms occurred in 1993. Our dataset includes a large number of events extending over the entire area of the western Alps, allowing us to get more stable results. Granet and Hoang Trong (1980) provide no information on their local magnitude computation.

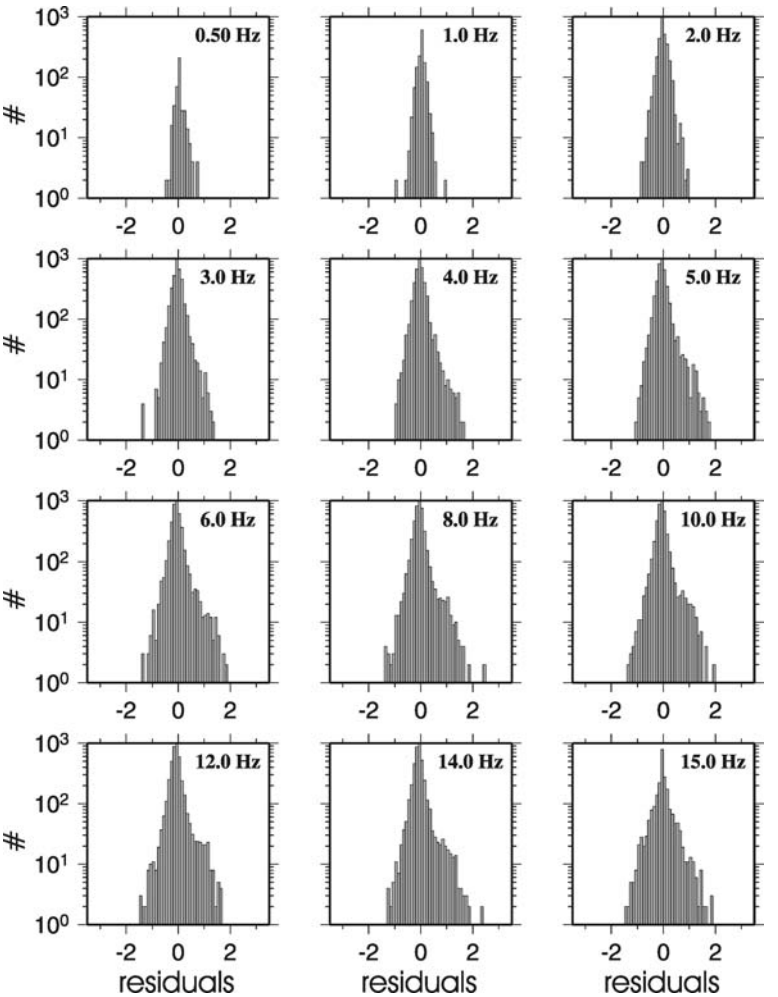

Fig. 11 Histograms of the residuals computed in the regressions over the peak amplitudes for each frequency. The use of an L1-norm minimization scheme eliminates the effects of the non-Gaussian large tails of residuals

Predicting the ground motion

That of the Western Alps is a low seismicity area, where the seismic hazard mainly depends on small-to-moderate earthquakes. In this section, we produce quantitative predictions of ground motion for earthquakes characterized by magnitudes up to M_w 5. Figure 13a shows the predicted curves for magnitude 4 and 5. The large amount of recordings from small earthquakes provides strong constraints on regional wave propagation, in fact, the estimated Peak Ground Acceleration (PGA) as a function of epicentral distance (Figure 13a) are obtained based on RVT, as implemented by Boore (1996), by using the attenuation parameters and the empirical duration function that are given in this study.

For magnitude 5, the predicted peak values are compared with those by Sabetta and Pugliese (1996), who regressed a very small accelerometric data set of strong-motion waveforms from events occurred in the Apennines, in Sicily, and in the eastern Alps. Comparisons are also given with the results by Ambraseys et al. (1996), who regressed the strong-motion data from the European accelerometric data set. At M 5, it is worth mentioning that the data set used by Sabetta and Pugliese spanned only the first 20 km from the seismic source. We used a uniform magnitude scale to take into account that Sabetta and Pugliese (1996) use local magnitude for $M < 5.5$ and Ms otherwise, while for Ambraseys et al. (1996) the reference magnitude is Ms. No distance conversion was necessary since Ambraseys et al. (1996) refer to fault distance only for magnitude >6. The comparison between different estimates of PGA for magnitude 5 (Figure 13a) shows interesting differences: except at small distances, our predicted ground motions are generally lower than

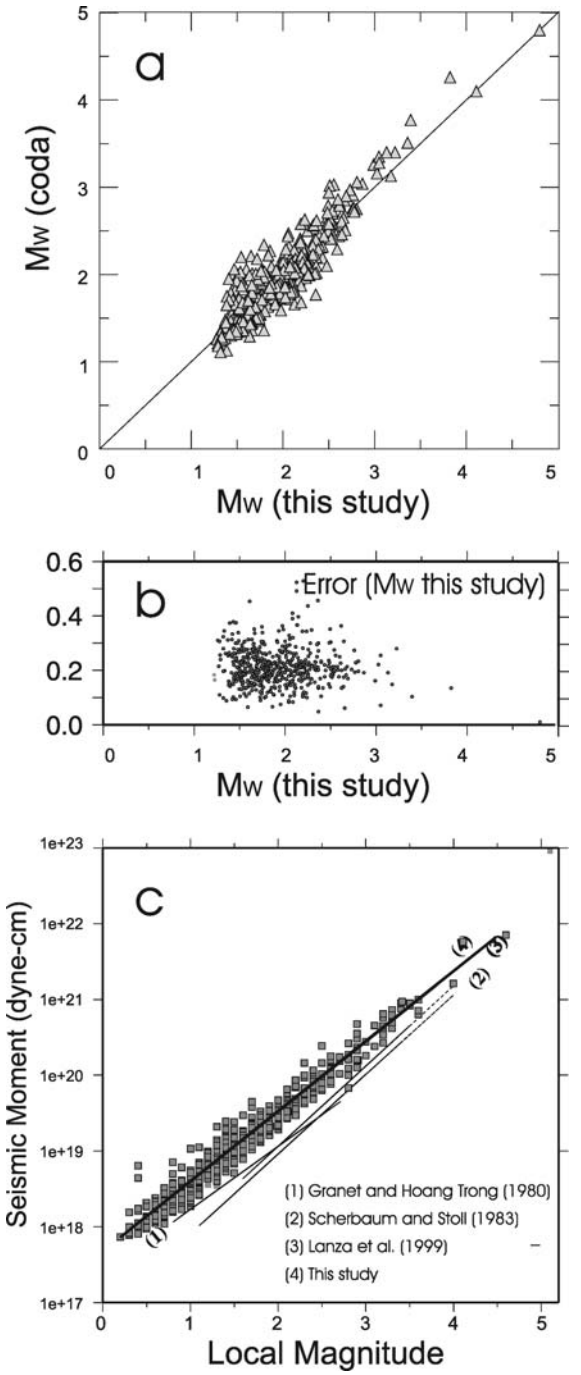

Fig. 12 (a) M_w derived from this study versus M_w(coda) given by Morasca et al. (2005). The values are in excellent agreement when we use $K = 0.24$. (b) The error associated to our M_W estimates is of the order of 0.2. (c) Our seismic moments versus M_L for all earthquakes in the data set (gray square symbols). Thick line is the least-squares fit to this data set; thin lines are the relationships for Friuli, NE Italy (Granet and Hoang Trong, 1980), Swabian Jura, SW Germany (Scherbaum and Stoll, 1983) and SW sector of Alps (Lanza et al., 1999)

both predictions by Sabetta and Pugliese (1996) and Ambraseys (1996). Keeping in mind that the data set used to calibrate the attenuation parameters for the Western Alps shows few events of magnitude >4, we could hypothesize that this could be one cause of the difference in the comparison. However, we should not neglect the fact that neither Ambraseys et al. (1996), nor Sabetta and Pugliese (1996), used events located in the western Alps.

In figure we plotted some observed PGA values obtained for the Asti earthquake (2000 August 21st, $M_W = 4.8$) confirming that the PGA values are lower for the Western Alps region than the values predicted by Sabetta and Pugliese (1996) and Ambraseys (1996). Their overestimations for magnitude 5 suggests that we should be careful in deriving ground motion parameters for moderate events using attenuation relationships calibrated using only large events. Moreover, regional differences in the attenuation of seismic waves should not be neglected because reflect differences in the geologic structures and in the thermal histories. For example, the Apennines are characterized by a strong attenuation, $Q(f) = 130 f^{0.1}$ (Malagnini et al., 2000a), which is caused by the presence of a high fracture density and consequently of large fluid/volatile flows in the crust; the attenuation of the seismic waves is lower in more stable portions of the crust, like that beneath Friuli (eastern Alps), $Q(f) = 260 f^{0.55}$ (Malagnini et al., 2002). The western Alps (in this study), where crystalline basement is shallower, has also a low-attenuation crust, $Q(f) = 310 f^{0.2}$. Differences in wave propagation can thus be easily linked with the geologic and tectonic settings of the areas and play a key role in hazard studies.

Spectral velocities are obtained for magnitude 4 and 5 and shown in Fig. 13b and c. Our results are compared at magnitude 5 with results of regressions carried out by Sabetta and Pugliese (1996) and by Ambraseys et al. (1996) for epicentral distances of 15 and 60 km. As for the PGA curves, we converted the different magnitude scale to moment magnitude. The figures show that our pseudo-velocity spectra are generally lower than those obtained by Ambraseys et al. (1996) and Sabetta and Pugliese (1996). The explanation is that our curves are the result of a careful calibration of attenuation parameters on moderate events recorded in the Western Alps region, whereas, in the other two studies, the parameters are calibrated using strong motion data from a

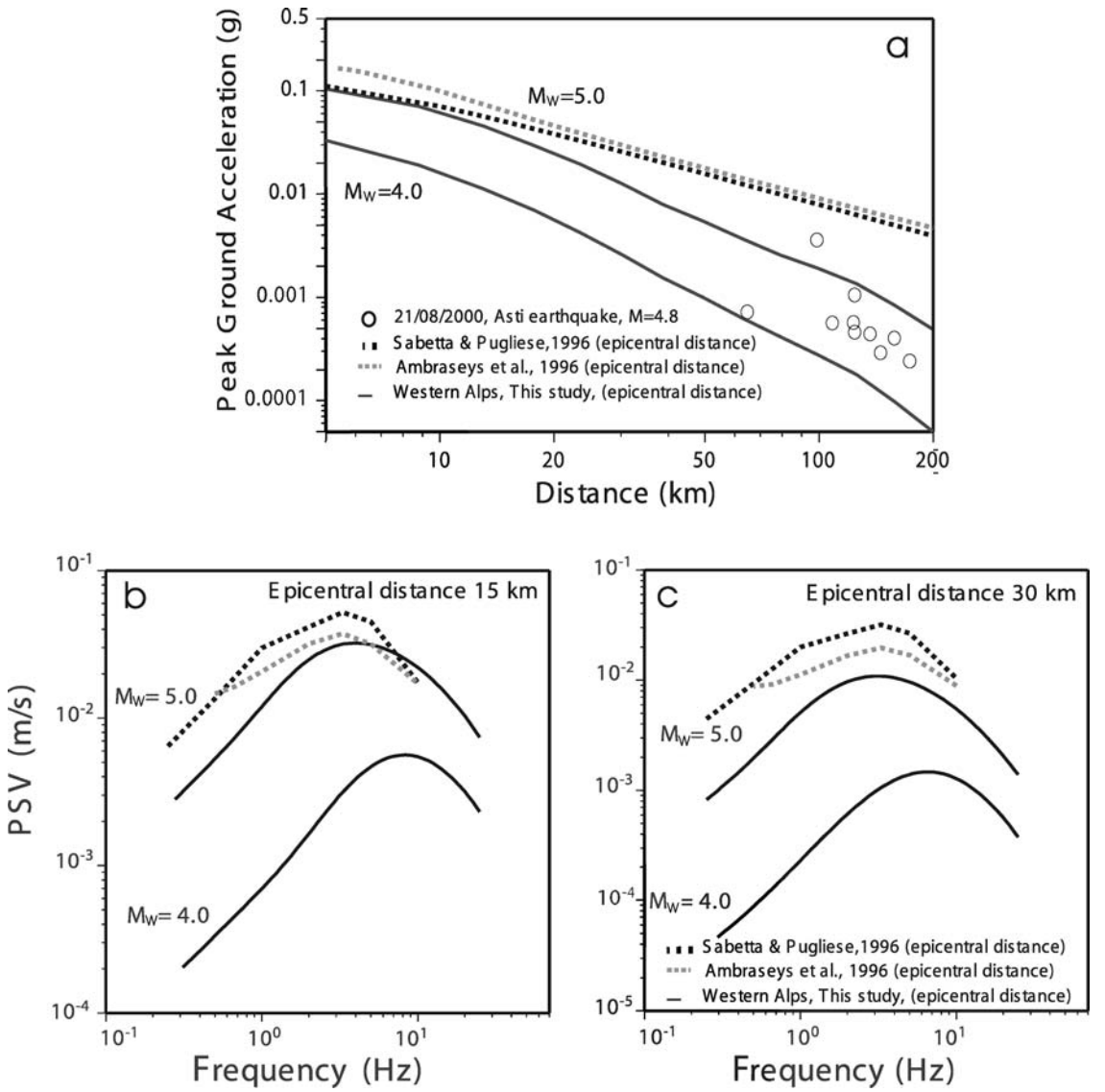

Fig. 13 (a) Our estimates of PGA (solid lines) computed for hard rock sites and based on the attenuation and excitation parameters obtained in this study. For $M_W = 5$ our curves are compared with the results of the regressions by Sabetta and Pugliese (1996, dashed curves) and Ambraseys et al. (1996) (dotted curves). Errors of 0.17 and 0.15 are associated to magnitude 5 and 4 respectively. (b, c) Our predicted response spectra relative to $M_W = 5$ and 4 (solid lines) at the fault distances of 15 (b) and 30 km (c). Our curve at magnitude 5 is compared with the empirical results of Sabetta and Pugliese (1996, dashed curves) and Ambraseys et al. (1996, dotted curves)

number of regions that are tectonically and geologically heterogeneous.

Conclusions

The main result of this study is the characterization of the regional attenuation in the western Alps that we describe by modeling the empirical results obtained inverting a large amount of data from the background seismicity within the region. The crustal propagation is described by a quadri-linear geometrical spreading within hypocentral distances of 160 km for frequencies up to 1.0 Hz, and by a simpler bilinear function at higher frequencies. The parameter $Q(f) = 310 f^{0.20}$ is used for taking into account the anelastic attenuation and indicates a fairly stable region.

By comparing our results with the ones obtained in similar studies (Bay et al., 2003; Malagnini et al., 2002), we observed, around 1.0 Hz, similar attenuation characteristics for the western Alps, the eastern Alps, and Switzerland. A much lower attenuation at high frequency characterize the eastern Alps, whereas the entire frequency band of engineering interest is affected by a much stronger attenuation in the Apennines.

The complex geometrical spreading reflects the average 1-D structure of the crust in the region, in terms of the depths of the most important interfaces, and of the impedance contrasts across them. Local earthquake tomography reveals the complexity of the three-dimensional lithospheric structure in the region (Kissling, 1993; Kissling and Spakman, 1996; Paul et al., 2001), suggesting the presence of asymmetric crustal roots, and of anomalous high-velocity features, like the Ivrea body (a wedge of Adriatic upper mantle, Paul et al., 2001).

The role of the three-dimensional complexities in determining the attenuation functional forms proposed in this study is still unclear: if the source-receiver geometry allows systematic effects, these may lead to changes in the apparent geometrical spreading function. If no systematic effects exist, lateral heterogeneities may only increase the amplitudes of the residuals. For the region investigated here, a preliminary analysis of the 2-D distribution of the residuals excludes systematic distributions of the residuals along specific paths. Moreover, the relative simplicity of the high-frequency attenuation relationships suggests the absence of systematic effects on the apparent attenuation itself.

The regression analysis produced other two interesting results:

1. a set of site terms that show some fluctuations with respect to the reference station STV2, located on hard rock. The larger site amplification is observed for station MONE in the frequency band 1–14 Hz. This relative site effect is coherent with observations by Spallarossa et al. (2002) and it is validated by the different geology between the two stations. Since for the other stations the shallow geology is poorly known, our results are an important contribution to have an idea of the site influence for future analysis on earthquakes recorded by RSNI network.
2. a suite of excitation terms (one for each earthquake included in the specific regression). For magnitudes larger than ∼4, and to the reference station STV2, we observed that the model require $\kappa_o = 0.012$ s, and maximum values for the stress parameter of 45–50 MPa.

A modeling effort was undertaken using the stochastic tool called Random Vibration Theory (Cartwright and Longuet–Higgins, 1956), in order to produce a predictive relationship of engineering interest (in terms of peak acceleration, spectral acceleration etc.). Differences in the predicted ground motions from our relationships and the existing ones (e.g., Ambraseys et al., 1996; Sabetta and Pugliese, 1996) arise because our results are based solely on information obtained from the specific region. On the contrary, the cited studies were carried out on heterogeneous data sets made of recordings of events within the entire Italian territory or even within Europe. Differences in the estimated peak ground accelerations from different studies in different tectonic and geologic environments (the Apennines, the eastern and the western Alps) show the importance of studying the basic factors (the source scaling, the regional attenuation and the site conditions) and their influences to the seismic hazard.

Finally the attenuation parameters obtained here allowed us to correct the recorded displacement spectra even for very small earthquakes, and to automatically compute precise estimates of seismic moments and moment magnitudes. This is a very important result, given the lower and the upper limits of the data distribution ($M_w \sim 1.3$ and $M_w \sim 4.8$), and could be used also for future events in the western Alps region.

Results have been validated through a comparison with stable estimates of moment magnitude obtained for the same dataset by Morasca et al. (2005). A systematic DC-shift between our results and those from other studies (Scherbaum and Stoll, 1983; Lanza et al., 1999; Granet and Hoang Trong, 1980) strongly suggests that magnitudes must be computed using relationships calibrated on the region of interest.

Acknowledgements

The authors wish to thank Prof. Claudio Eva and the RSNI network staff (G. Carenzo, M. Pasta and E.

Zunino) for the careful network management and data collection that made this work possible. We are also indebted to the Editor, E. Faccioli and to the anonymous reviewers, that provided valuable comments that significantly improved the original manuscript.

This work has been partially supported by the *Ministero dell'Universita' e della Ricerca Scientifica (MIUR)*, through project FIRB prot. RBAU013NRZ.

References

Ambraseys NN, Simpson KA, Bommer JJ (1996) Prediction of horizontal response spectra in Europe. Earthquake eng Struct Dyn 25:371–400

Atkinson GM, Boore DM (1995) Ground motion relations for Eastern North America. Bull Seism Soc Am 85(1):17–30

Atkinson GM, Silva WJ (1997) An empirical study on earthquake source spectra. Bull Seism Soc Am 87:97–118

Bay F, Fäh D, Malagnini L, Giardini D (2003) Spectral shear-wave ground-motion scaling in Switzerland. Bull Seism Soc Am 93(1):414–429

Boore DM (1983) Stochastic simulation of high-frequency ground motions based on seismological models of the radiated spectra. Bull Seism Soc Am 73(6):1865–1894

Boore DM (1996) SMSIM – Fortran programs for simulating ground motion from earthquakes: version 1.0. U. S. Geological Survey open – file report 96-80-A:73

Boore DM (2000) Prediction of ground motion using the stochastic method. Aki Symposium, PAGEOPH, v 1.1

Boore DM, Boatwright J (1984) Average body-wave radiation coefficients. Bull Seism Soc Am 74:1615–1621

Boore DM, Joyner WB, Fumal ET (1997) Equations for estimation horizontal response spectra and peak acceleration from western North American earthquakes: a summary of recent work. Seis Res Lett 68(1):129–154

Brune JN (1970) Tectonic stress and the spectra of seismic shear waves from earthquakes. J Geophys Res 75:4997–5009

Buness H, Giese P, Hirn A, Nadir S, Scarascia S (1990) Crustal structure derived from seismic refraction between Southern Alps and the Ligurian Sea. Proceeding of the sixth workshop on the EGT project: data compilation and synoptic interpretation, edited by Freeman R, Mueller St, European Science Foundation, Strasbourg, France, pp 165–167

Campbell WK (1997) Empirical near-source attenuation relationships for horizontal and vertical components of peak ground acceleration, peak ground velocity, and pseudo absolute acceleration response spectra. Seism Res Lett 68(1):128–154

Cartwright DE, Longuet-Higgins MS (1956) The statistical distribution of the maxima of a random function. Proc Roy Soc London A 237:212–232

Castaldini D, Panizza M (1991) Inventario delle faglie attive tra i fiumi Po e Piave e il Lago di Como (Italia settentrionale). Il Quaternario 4:605–611

Castro RR, Pacor F, Sala A, Petrungaro C (1996) S-wave attenuation and site effects in the region of friuli, Italy. J Geophys Res 101:22355–22369

Cattaneo M, Augliera P, Parolai S, Spallarossa D (1999) Anomalously deep earthquakes in northwestern Italy. Journal of Seismology 3(4):421–435

Castellarin A (2001) Alps-appennines and Po plain-frontal appennines relations. In Vai GB, Martini IP (eds) Anatomy of an orogen: the apennines and adjacent mediterranean basins. Kluwer Academic Publishers, Dordrecht-Boston-London, pp 177–196

CNR-PFG (1987) Neotectonic map of Italy. Quaderni de La Ricerca Scientifica:114

Console R, Rovelli A (1981) Attenuation parameters for friuli region, from strong-motion acelerogram spectra. Bull Seism Soc Am 71:1981–1991

Dal Piaz GV (1995) Plate tectonics and mountain building: the Alps. historical review and personal comments. In: Ranalli G (ed) Proceedings VIII Summer School Earth & Planetary Sci., Plate Tectonics: The first twenty-five years, Univ. Siena 1994, pp 171–251

Dewey JF, Pitman WC, Ryan WBF, Bonnin J (1973) Plate tectonics and the evolution of the alpine system. Bulletin Geo Soc Am 84:3137–3180

Di Stefano R, Chiarabba C, Lucente F, Amato A (1999) Crustal and uppermost mantle structure in Italy from the inversion of P-wave arrival times: geodynamic implications. Geophys J Int 139:483–498

Eva C, Cattaneo M, Augliera P, Pasta M (1991) Regional coda Q variations in the western Alps (northern Italy). Phys Earth Planet Inter 67:76–86

Eva E, Solarino S (1998) Variations of stress directions in the western Alpine arc. Geophis J Int 135:438–448

Ferrari G (1991) The 1887 Ligurian earthquake: a detail study from contemporary scientific observations. Tectonophysics 93:131–139

Galadini F, Meletti C, Vittori E (2001) Major active faults in Italy: available surface data. Netherlands Journal of Geosciences 80:273–296

Giglia G, Capponi G, Crispini L, Piazza M (1996) Dynamics and seismotectonics of the West-Alpine arc. Tectonophysics 267:143–175

Granet M, Hoang Trong P (1980) Some medium properties at Friuli (Italy) from amplitude spectrum analysis: a possible change in time or in space. Tectonophysics 68:16–182

Herrmann RB, Malagnini L (2005) Interpretation of high frequency ground motion from regional seismic network observations. Bull Seism Soc Am (submitted)

Kissling E (1993) Deep structure of the Alps – what do we really know? Physics of the Earth and Planetary Interiors 79:87–112

Kissling E, Spakman W (1996) Interpretation of tomographic images of uppermost mantle structure: examples from the western and central Alps. J Geodynamics 21(1):97–111

Lanza V, Spallarossa D, Cattaneo M, Bindi D, Augliera P (1999) Source parameters of small events using constrained deconvolution with empirical Green's functions. Geophis J Int 137: 651–662

Malagnini L, Akinci A, Herrmann RB, Pino NA, Scognamiglio L (2002) Characteristics of the ground motion in northeastern Italy. Bull Seism Soc Am 92(6):2186–2204

Malagnini L, Herrmann RB (2000) Ground motion scaling in the region of the Umbria-Marche earthquake of 1997. Bull Seism Soc Am 90:1041–1051

Malagnini L, Herrmann RB, Di Bona M (2000a) Ground motion scaling in the apennines (Italy). Bull Seism Soc Am 90:1062–1081

Malagnini L, Herrmann RB, Koch. K (2000b) Regional ground-motion scaling in central Europe. Bull Seism Soc Am 90:1052–1061

Malagnini L, Mayeda K, Akinci A, Bragato PL (2004) Estimation absolute site effects. Bull Seism Soc Am 94(4):1343–1352

Morasca P, Mayeda K, Malagnini L, Walter WR (2005) Coda derived source spectra, moment magnitudes, and energy-moment scaling in the Western Alps. Geoph J Int 160(1):263–275

Paul A, Cattaneo M, Thouvenot F, Spallarossa D, Béthoux N, Fréchet J (2001) A three-dimensional crustal velocity model of the southwestern Alps from local earthquake tomography. J Geophis Res 106(B9):19367–19389

Polino R, Gosso G, Dal Piaz GV (1990) Un modello attualistico sulla genesi delle Alpi. Memorie della Società Geologica Italina 45:71–75

Sabetta F, Pugliese A (1996) Estimation of response spectra and simulation of nonstationary earthquake ground motion. Bull Seism Soc Am 86:337–352

Sadigh K, Chang CY, Egan JA, Makdisi F, Youngs RR (1997) Attenuation relationship for shallow crustal earthquakes based in California strong motion data. Seism Res Lett 68:154–180

Scherbaum F, Stoll D (1983) Source parameters and scaling laws of the 1978 Swabian Jura (southwest Germany) aftershocks. Bull Seism Soc Am 73:1321–1343

Scognamiglio L, Malagnini L, Akinci A (2005) Ground motion scaling in Eastern Sicily (Italy). Bull. Seism Soc Am 95(2):568–578

Spallarossa D, Bindi D, Augliera P, Cattaneo M (2002) An M_L scale in Northwestern Italy. Bull Seism Soc Am 92(6):2205–2216

Sue C, Thouvenot F, Fréchet J, Tricart P (1999) Earthquake analysis reveals widespread extension in the core of the Western Alps. J Geophys Res 104:25611–25622

Sue C, Tricart P (1999) Late-alpine brittle extension above the frontal pennine thrust near Briançon, Western Alps. Eclog Geol Helv 92:171–181

Thouvenot F (1983) Frequency dependence of the quality factor in the upper crust: a deep seismic sounding approach. Geophys J R Astr Soc 73:427–447